Proceedings of the 28th IEEE
EMBS Annual International Conference
New York City, USA, Aug 30-Sept 3, 2006

A Comparison of Adaptive and Non-Adaptive EEG Source Localization Algorithms Using a Realistic Head Model

John P. Russell, Zoltan J. Koles, *Member, IEEE*

***Abstract*—An accurate and robust electroencephalogram (EEG) source localization algorithm would be a definite asset for the surgical treatment of patients with epilepsy. Due to the underdetermined nature of the EEG inverse problem, a variety of algorithms with unique constraints and assumptions are applied to select the current dipole source distribution that best accounts for the scalp recordings. We investigated four algorithms: two non-adaptive algorithms: the minimum norm and LORETA as well as two adaptive algorithms: the Borgiotti-Kaplan and eigenspace projection beamformers. Compared over a range of SNR values and single source locations, we found that the eigenspace projection beamformer exhibited superior localizing capabilities compared to the other three algorithms while minimizing source current dispersion. The size of the data window required to accurately localize using the adaptive beamformers was also investigated to improve algorithm efficiency and minimize stationary source assumptions.**

I. Introduction

Epilepsy is a recurrent seizure-related disorder of the central nervous system that affects approximately 1% of the population. A seizure occurs when there is an increase in the synchronous behavior of a localized group of pyramidal cells within the cerebral cortex resulting in a surge of electrical activity. The over-stimulation at the seizure focus irritates neighboring regions causing the seizure to spread. Some forms of epilepsy may be treated with medication while other types are medically intractable. For the latter cases, a suitable treatment option is to surgically remove the seizure focus. Therefore, a robust and accurate algorithm for localizing the seizure focus is necessary for successful surgical treatments. The location of the focus is estimated using ictal electroencephalogram (EEG) scalp potentials in a variety of pseudo-inverse methods. We will compare the localizing capabilities of four inverse methods: minimum norm (MN), low resolution brain electromagnetic tomography (LORETA), Borgiotti-Kaplan beamformer, and the eigenspace projection beamformer using a realistic head model.

II. Background Information

The forward problem maps the internal source current density vector, **j**(t), within the cortex to the EEG potentials measured at N electrode sites on the scalp, **v**(t), via a geometrical and anatomical dependent conductivity map known as the lead field matrix, **K.**

$$\mathbf{v}(t) = \mathbf{K}\mathbf{j}(t) \qquad (1)$$

The solution space consists of M current dipole sources evenly distributed throughout the grey matter of the head model. Each dipole may have a different magnitude and orientation.

Source localization attempts to determine the inverse solution to (1) using **v**(t), a measurable quantity, to estimate **j**(t). This process yields estimations for the magnitude and orientation of each current dipole source. Due to the severely underdetermined nature of this problem (M >>N), there are multiple solutions for **j** that yield identical scalp potentials. Therefore, physiological and anatomical à priori knowledge is used to isolate the most probable inverse solution.

A. Non-adaptive spatial filters

The MN and LORETA pseudo inverse methods are non-adaptive spatial filters whose estimates of $\mathbf{K}^{-1}$, are calculated independently of the measured scalp potentials. The MN algorithm constrains estimated source current density, $\hat{\mathbf{j}}$ by minimizing the solution's overall power [1]:

$$\min_{\hat{\mathbf{j}}} \left(\hat{\mathbf{j}}^T \hat{\mathbf{j}} \right), \text{ subject to } \mathbf{v} = \mathbf{K}\mathbf{j} \qquad (2)$$

The solution to (2) is:

$$\hat{\mathbf{j}} = \mathbf{T}\mathbf{v} \text{ where } \mathbf{T} = \mathbf{K}^T \left[\mathbf{K}\mathbf{K}^T \right]^{-1} \qquad (3)$$

MN introduces bias into the estimated current solution by pulling sources towards electrode sites to minimize total power. The validity of the physiological assumption of minimum power also comes into question [2].

LORETA introduces a weighting matrix **W** into the aforementioned MN solution. **W** incorporates a 3D high pass spatial filter to achieve a maximally smooth estimated current density to emphasize the correlated nature of neighboring pyramidal cells. **W** also contains a depth

Manuscript received April 24, 2006. This work was supported in part by National Sciences and Engineering Research Council of Canada under Grant G121210951.

John P. Russell and Zoltan J. Koles are with the University of Alberta, Edmonton, AB T6G 2E1, Canada (phone: 780-492-9463; e-mail: jpr2@ualberta.ca, z.koles@ualberta.ca).

weighting matrix to offset the bias introduced in MN. The LORETA pseudo inverse, **T** is [1]:

$$\mathbf{T} = \mathbf{W}^{-1}\mathbf{K}^T\left[\mathbf{K}\mathbf{W}^{-1}\mathbf{K}^T\right]^+ \quad (4)$$

+ denotes the Moore-Penrose pseudo inverse [1].

The smoothing process in LORETA results in a blurring of the solution. The volume of the solution space in which correlated behavior can be correctly assumed introduces additional error [3].

B. Adaptive spatial filters

Beamformers are spatial filters used to estimate activity at a specific location by suppressing interference originating elsewhere [3]. Intuitively speaking, beamforming algorithms perform a scan of the entire solution space with a 'virtual' electrode in order to estimate each voxels contribution to the measured output. Weights are derived from the covariance matrix, **R**, of the measured data, **v**(t). Each voxel in the solution space has three unique weights; one for each orthogonal direction. Given this, the amplitude of the current source dipole at location **r**, with orientation **η**, at time t is [4]:

$$\hat{j}(\mathbf{r},\eta,t) = \mathbf{w}^T(\mathbf{r},\eta)\,\mathbf{v}(t) \quad (5)$$

The weights **w**, in (5) can be calculated using a variety of constraints. The two beamformers under investigation here are the Borgiotti-Kaplan beamformer and the eigenspace projection beamformer. Both are extensions of the linearly-constrained minimum-variance beamformer [5]. The Borgiotti-Kaplan beamformer minimizes the overall estimated current density while providing unity white noise gain [4]:

$$\min_{\mathbf{w}_x}\left(\mathbf{w}_x^T\mathbf{R}\mathbf{w}_x\right), \text{ constrained by:}$$
$$\mathbf{w}_x^T\mathbf{w}_x = 1,\ \mathbf{w}_x^T\mathbf{k}_y(\mathbf{r}) = 0, \text{ and } \mathbf{w}_x^T\mathbf{k}_z(\mathbf{r}) = 0 \quad (6)$$

$\mathbf{k}_i(\mathbf{r})$ is a single column of lead field matrix, **K**, corresponding to the conductivities between a voxel, with location **r** oriented in the i direction, and each electrode. Similar optimizations apply for $\mathbf{w}_y$ and $\mathbf{w}_z$. The minimization equations (6) are solved using the Lagrange multiplier method [4] yielding:

$$\mathbf{w}_\eta = \frac{\mathbf{R}^{-1}\mathbf{k}(\mathbf{r})\left[\mathbf{k}^T(\mathbf{r})\mathbf{R}^{-1}\mathbf{k}(\mathbf{r})\right]^{-1}\mathbf{f}_\eta}{\sqrt{\mathbf{f}_\eta^T\Omega\mathbf{f}_\eta}} \quad (7)$$

Where $\mathbf{f}_\eta$ is the unit vector of **η** and

$$\Omega = \left[\mathbf{k}^T(\mathbf{r})\mathbf{R}^{-1}\mathbf{k}(\mathbf{r})\right]^{-1}\mathbf{k}^T(\mathbf{r})\mathbf{R}^{-2}\mathbf{k}(\mathbf{r}) \cdot\left[\mathbf{k}^T(\mathbf{r})\mathbf{R}^{-1}\mathbf{k}(\mathbf{r})\right]^{-1} \quad (8)$$

The weights form a signal pass-band at the voxel of interest and stop-bands elsewhere. Due to the limitations imposed by the degrees of freedom, a solution space wide stop-band is unattainable. Therefore, the stop-bands are focused over voxels emitting significant power [5].

The eigenspace projection beamformer projects the weights derived in (7) onto the eigenvectors of **R** of maximum variance, or power. The weights are given by:

$$\tilde{\mathbf{w}}_\eta = \mathbf{E}_R\mathbf{E}_R^T\mathbf{w}_\eta \quad (9)$$

$\mathbf{E_R}$ contains the 'maximum variance' eigenvectors of **R**

For optimal results, the number of sources should be known à priori so that the corresponding number of eigenvectors are included in $\mathbf{E_R}$. This method improves the SNR of the beamformer output as shown in [6].

Both beamformers produce erroneous results with multi-source configurations experiencing some degree of correlation because the covariance matrix can no longer discriminate between the correlated portions of the two sources. This may result in the suppression of the two correlated sources and the formation of a phantom source located elsewhere [4].

III. Simulations and Results

A. Single source localization

T1 weighted MR images of a human head were segmented onto a 1 mm^3 regular grid using a semi-automatic dynamic edge tracer segmentation algorithm into 6 861 888 voxels consisting of cerebellum, cortex, cerebral spinal fluid, white matter, skull, and scalp [7]. The solution space was defined as a single layer of continuous cortex discretized into M = 78 433 voxels.

A single 17 Hz sinusoidal dipole source was placed at random locations within the solution space and oriented normally to the cortical surface. The scalp potentials were calculated using (1) for a N = 32 electrode configuration with a left ear reference. The lead field matrix for the solution space was obtained using the finite volume method [8]. The EEG output, **v**(t), was sampled at 256 Hz.

Gaussian white noise was added to **v**(t) yielding SNR values of 10, 5, and 2. The SNR was defined as the ratio of the sum of the eigenvalues of the signal covariance matrix and the sum of the eigenvalues of the noise covariance matrix. The noise values are consistent with the lower, middle, and upper values estimated with a phantom human head [9]. The added noise alleviates the difficulties in inverting the ill-

conditioned covariance matrix. 100 trials were performed at each SNR value with 256 samples of the EEG used in the calculation of **R**.

Localizing error was calculated by comparing the location of the peak of the estimated current density versus the actual source location.

TABLE I
LOCALIZING ERRORS (mm)

	SNR = 10	SNR = 5	SNR = 2
MN	66.09 ± 37.60	71.60 ± 34.91	78.30 ± 33.48
LORETA	67.09 ± 37.32	70.77 ± 34.47	80.10 ± 33.47
BK beam	5.46 ± 19.09	6.63 ± 20.10	13.07 ± 28.60
ES beam	0.54 ± 0.78	0.88 ± 0.89	1.82 ± 2.19

Results represented as mean ± standard deviation for 100 trials

Both beamformers exhibit superior localizing capabilities in comparison to the non-adaptive spatial filters. The eigenspace projection beamformer performs significantly better than the other three algorithms and displays robustness to increasing noise levels (see Fig. 1). The superior performance of the eigenspace projection beamformer is expected due to the additional à priori knowledge utilized by the eigenspace beamformer during weighting derivations. Realizing a single source experiment, the weights were projected onto a one dimensional signal subspace determined by the eigenvector of **R** corresponding to the greatest source of signal power. The eigenspace projection and Borgiotti-Kaplan beamformers experienced their largest localizing errors with sources located near the base of the cortex as well as locations buried deep within sulci.

To illustrate the electrode bias introduced by the non-adaptive filters and the electrode bias resiliency of the beamformers, the location of the actual and estimated sources were measured with respect to electrode locations. The mean distance from the actual source to each of the 32 electrodes was compared to the same measure of the estimated maximum. A positive value represents a move to a more 'electrode dense' location that would reduce the overall power of the distributed source model.

TABLE II
QUANTIFYING ELECTRODE BIAS (mm)

	SNR = 10	SNR = 5	SNR = 2
MN	2.48 ± 2.90	2.61 ± 2.97	2.98 ± 3.09
LORETA	2.38 ± 2.75	2.35 ± 2.97	2.87 ± 3.09
BK beam	0.04 ± 1.11	0.12 ± 0.65	0.03 ± 1.56
ES beam	0.00 ± 2.81	-0.01 ± 2.81	0.00 ± 2.81

Results represented as mean ± standard deviation for 100 trials

Table II illustrates the bias that the electrode configuration produces on the inverse solutions of non-adaptive spatial filters.

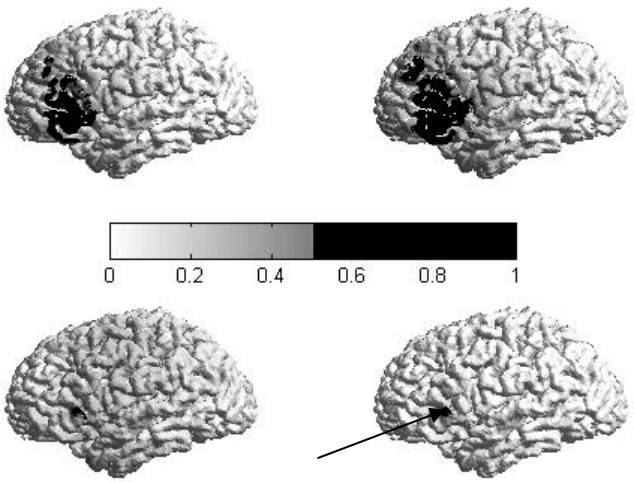

Fig. 1. Example of estimated current densities with SNR = 5. Darker regions represent increased source power. Top left = MN, top right = LORETA, bottom left = Borgiotti-Kaplan beamformer, bottom right = eigenspace projection beamformer. Actual source location is marked with arrow.

Due to the nonsymmetrical nature of the solution space and the resulting estimated current density, the full-width half-maximum of the estimated current density was quantified via:

$$dispersion = \sqrt{\sum_{N} \hat{j}(\mathbf{r})(\mathbf{r}-\mathbf{r}_{\max})^2} \qquad (10)$$

N is the number of voxels with a dipole magnitude greater or equal to $0.5\,\hat{j}_{\max}$. The location of the estimated current density peak is $\mathbf{r}_{max}$. For the calculation of the dispersion in (10), $\hat{\mathbf{j}}$ is normalized so that $\hat{j}(\mathbf{r}_{\max}) = 1$.

TABLE III
ESTIMATED CURRENT DISTRIBUTION DISPERSION (mm)

	SNR = 10	SNR = 5	SNR = 2
MN	1545 ± 1066	1443 ± 942	1160 ± 781
LORETA	1917 ± 1593	1644 ± 1309	1402 ± 989
BK beam	46 ± 54	179 ± 498	1061 ± 1769
ES beam	33 ± 27	59 ± 46	145 ± 110

Results represented as mean ± standard deviation for 100 trials

It is anatomically known that the pyramidal cells within the gray matter are oriented normally to the surface of the cortex [10]. This additional à priori knowledge was utilized in a second experiment where estimated current source dipole magnitudes and orientations were projected on to the normal vector of each voxel. The normal vectors corresponded to the unit vector of minimal grey matter thickness at each voxel. Differences in peak localizing error for all four algorithms were minimal, with slight improvements for the normally projected current source distribution. The dispersion, as calculated in (10), was greatly reduced for all four algorithms.

TABLE IV
ESTIMATED CURRENT DISTRIBUTION DISPERSION (mm)

WITH NORMAL VECTOR PROJECTION

	SNR = 10	SNR = 5	SNR = 2
MN	796 ± 491	782 ± 511	618 ± 409
LORETA	901 ± 739	794 ± 647	686 ± 492
BK beam	25 ± 26	99 ± 288	595 ± 928
ES beam	18 ± 15	31 ± 25	73 ± 54

Results represented as mean ± standard deviation for 100 trials

B. The Covariance Matrix

The robustness of the covariance matrix used in beamforming algorithms is dependent on the number of samples used to calculate **R**. If too few samples are used, spurious positive correlation indications may result. Conversely, too many samples are computationally burdensome and assumptions of source stationarity could be violated.

To determine the minimum number of samples necessary to obtain a robust estimate of **R**, a single source was localized using both aforementioned beamforming techniques with a SNR = 5. The number of samples used to calculate **R**, ranged from 1 to 256 in single increments. 10 trials were conducted at each increment. Even with the addition of random noise to the measurement data, **R** will be a nonsingular matrix as long as the number of observations (electrodes) exceeds the number of the samples utilized in calculating **R** [5]. Therefore, a regularization factor was implemented with 1% of the largest eigenvalue added along the diagonal of the **R** to ensure stable inversion.

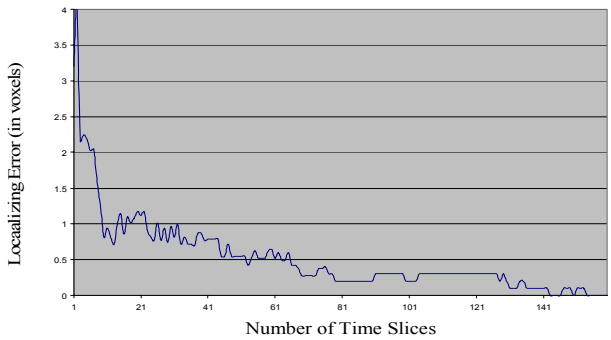

Fig. 2. Localizing error using the eigenspace projection beamformer versus the number of time slices used to estimate the covariance matrix **R**. SNR = 5. The response for the Borgiotti-Kalpan beamformer was identical to the eigenspace projection beamformer and was therefore omitted from the figure.

Fig. 2 illustrates that localizing error given the aforementioned specifications approaches zero with approximately 150 samples. This is equivalent to just over 0.5 sec of data required for the estimation of **R**.

IV. Discussion

The complexity of the realistic-head solution space tends to amplify the known biases of an inverse solution, in particular the difficulties in localizing deeper sources. As shown, the adaptive spatial beamforming filters are more flexible to localizing sources in a variety of locations and are more immune to the effects of noise. The eigenspace projection beamformer proved to be the most accurate while minimizing blurring, but also required the most à priori knowledge related to the number of sources underlying the EEG. This is a luxury that may not be present when analyzing real EEG data.

Projecting the current source distribution onto the normal vectors of the solution space reduces the dispersion and lessens the effects of noise.

The major disadvantage of the beamformer is the computational complexity involved in calculating the weighting vectors. While a non-adaptive pseudo inverse, **T**, can be derived based on the properties of the solution space, the beamforming weighting vectors, $\mathbf{w}(\mathbf{r},\boldsymbol{\eta})$ must be continually updated based on the changing covariance structure of the measured data.

Future work will include variations of the eigenspace projection beamformer where the solution subspace will be chosen via independent component analysis and eigenvectors representing maximum variation between ictal and non-ictal EEG recordings.

V. References

[1] Pascual-Marqui RD, Review of methods for solving the EEG inverse problem *International Journal of Bioelectromagnetism*, vol. 1, pp. 75-86, 1999.

[2] Michel CM, M. M. L. G. G. S. S. L., EEG source imaging *Clinical Neurophysiology*, vol. 115, pp. 2195-2222, 2004.

[3] Baillet S, M. J. L. R., Electromagnetic brain mapping *IEEE Signal Processing Magazine*, vol. 18, pp. 14-30, 2001.

[4] Sekihara K, N. S. P. D. M. A. M. Y., Reconstructing spatio-temporal activities of neural sources using an MEG vector beamformer technique *IEEE Transactions on Biomedical Engineering*, vol. 48, pp. 760-771, 2001.

[5] Van Veen, B. D., van Drongelen, W., Yuchtman, M., and Suzuki, A., Localization of brain electrical activity via linearly constrained minimum variance spatial filtering *IEEE Trans Biomed Eng*, vol. 44, pp. 867-80, Sep, 1997.

[6] Sekihara K, N. S. Neuromagnetic source reconstruction and inverse modeling. In: *Modeling and Imaging of Bioeectric Activity - Principles and Applications*, Anonymous Kluwer Academic/Plenum Publishers, 2004.pp. 213-250.

[7] Withey D, Dynamic Edge Tracing: Recursive Methods for Medical Image Segmentation, PhD Dissertation 2006. University of Alberta.

[8] Neilson, L. A., Kovalyov, M., and Koles, Z. J., A computationally efficient method for accurately solving the EEG forward problem in a finely discretized head model *Clin Neurophysiol*, vol. 116, pp. 2302-14, Oct, 2005.

[9] Leahy RM, M. J. S. M. H. M. L. J., A study of dipole localization accuracy for MEG and EEG using a human skull phantom *Electroencephalogr Clin Neurophysiol*, vol. 107, pp. 159-73, 1998.

[10] Martin JH. The Collective Electrical Behavior of Cortical Neurons: The Electroencephalogram and the Mechanisms of Epilepsy. In: *Principles of Neural Science*, Norwalk, Connecticut, USA: Appleton & Lange, 1991.pp. 777-791.